# Role of composition, site ordering, and magnetic structure for the structural stability of off-stoichiometric $Ni_2MnSb$ alloys with excess Ni and Mn

Sheuly Ghosh* and Subhradip Ghosh†
*Department of Physics, Indian Institute of Technology Guwahati, Guwahati-781039, Assam, India*

(Received 15 October 2018; revised manuscript received 15 January 2019; published 25 February 2019)

Using density-functional-theory-based calculations, we explore the factors that influence the phase stability of Ni and Mn excess off-stoichiometric $Ni_2MnSb$ alloys which have lately been proven to possess properties important for state-of-the art technology. Our calculations and subsequent analysis of the electronic structures pinpoint the origin of the behavior of phase stability in Ni-Mn-Sb systems. We find that the site occupancy patterns and subsequent magnetic structures are the key toward effecting a martensitic phase transformation. Our results demonstrate that apart from $Ni_2Mn_{1+x}Sb_{1-x}$ systems which have been experimentally observed to possess magnetic shape memory effect, $Ni_{2+x}MnSb_{1-x}$ too are potential shape memory alloys where an unexpected site occupancy configuration leading to reduction of total energy drives the martensitic phase transformation. This, thus, opens more possibilities for the experimentalists to explore new materials for magnetic shape memory and associated functional effects. The systems, irrespective of composition, are found to be ductile, a necessity for practical applications.

DOI: 10.1103/PhysRevB.99.064112

## I. INTRODUCTION

Magnetic shape memory alloys (MSMAs) have raised intense interest in recent years as multifunctional materials due to their diverse physical properties, such as magnetic shape memory, magnetocaloric, magnetic superelastic effects, magnetoresistance, and exchange bias. Among different MSMAs, Ni-Mn-Z (Z=Ga, In, Sn, Sb) are of special interest nowadays due to the existence of magnetostructural and metamagnetostructural phase transitions leading to their unique properties [1–15] and thus making them promising for applications in various engineering devices. The first-order martensitic phase transition (MPT) from a high-temperature $L2_1$ parent austenite phase to a low-temperature tetragonal or orthorhombic martensite phase associated with a change in magnetization in these alloys is very important, resulting in many exotic properties.

Unlike in the Ni-Mn-Ga family, the prototype MSMA, other Ni-Mn-Z (Z=In, Sn) alloys in Heusler structures undergo MPT and exhibit functional properties associated only in off-stoichiometric compositions and with systems substantially Z-deficient [16–20]. A recent addition to this class is the off-stoichiometric Sb-deficient Ni-Mn-Sb systems where magnetostructural transitions and significant magnetocaloric effect are observed near room temperature [21,22]. This, along with the low cost of Sb and achievable negligible hysteresis loss [23], makes Ni-Mn-Sb systems potential candidates for refrigeration and actuator applications. Extensive experimental investigations have revealed that MPT and associated properties in Ni-Mn-Sb alloys are dependent on the concentration ratio of Ni, Mn, and Sb. The martensitic transformation is observed in $Ni_2Mn_{1+x}Sb_{1-x}$ alloys for $x \geqslant 0.4$ [24]. Complex magnetic structures with short-range correlations are also inferred. The observed decrease of magnetic moment with increasing electron-atom ratio $e/a$; a behavior opposing the general trend in Heusler and semi-Heusler alloys, is attributed to the presence of these antiferromagnetic correlations. Similar features are observed by Khan *et al.* [25]. Experiments on systems with low Sb concentration (between 0.44 and 0.48) with either Ni content being fixed [15,22] or varying in a way to make the system Ni-deficient [23,25], observed significant Inverse magnetocaloric effect and exchange bias. All these experimental results pointed toward the presence of substantial antiferromagnetic interactions present due to an excess amount of Mn occupying presumably the Sb sites.

Although the experiments wonderfully established the potential multifunctional traits in Ni-Mn-Sb systems, certain fundamental questions remain to be answered. The systems that were investigated were always Sb-deficient and Mn-excess. This propels one to examine the role of composition on the properties, in particular the impact on the stabilities of the high-temperature austenite and the low-temperature martensite phases. Coupled with this is the question regarding the impact of site ordering in the system on the physical properties. Previous studies on off-stoichiometric Ni-Mn-Z (Z=Sn, Ga, In) showed that in the off-stoichiometric compositions, the excess atom does not always prefer to occupy the deficient atom site. The magnetic structure, as a consequence of this, also plays an important role in deciding the phase stability and the associated properties. For example, Hu *et al.* [26] showed that, for most of the off-stoichiometric $Ni_2MnGa$, though the excess atoms of the rich component occupy the deficient atom sites; for Ga-rich alloys, the excess Ga atoms always prefer the Mn sites no matter whether the system is Mn-deficient or not. For Ni-deficient Ga-excess $Ni_2MnGa$

*sheuly.ghosh@iitg.ac.in
†subhra@iitg.ac.in

 

systems, some of the Mn atoms move to the Ni sites and the excess Ga atoms occupy the Mn sites. For $Ni_2Mn_{1+x}Sn_{1-x}$, it was shown that the experimental phase diagram for Curie temperature can be verified only when an intermixing of Mn and Sn atoms is considered [27]. Li *et al.* [28] suggested a possibility of Mn-In ordering for Mn-excess off-stoichiometric $Ni_2Mn_{1+x}In_{1-x}$ compositions. They showed that magnetic ordering in the system can affect the MPT significantly. It was found that if there is ferromagnetic coupling between the Mn atoms at Mn site and In site, then no MPT occurs; whereas for antiferromagnetic coupling, MPT occurs in the system. For $Mn_2Ni_{1+x}Sn_{1-x}$ [29] also, an intricate relation between the site occupancy, magnetic ordering, and the stability of the martensite phase was observed. Thus, a knowledge of the site-occupancy will be essential for Ni-Mn-Sb systems to investigate the physical properties. Also, detailed and systematic investigation about the effects of site ordering and magnetic structure on phase stability for compositions beyond those considered in the experiments would help us understand the fundamental physics of the system and help choose the composition ranges where practical applications are most suitable.

Since relative stabilities of phases are central toward other features of this system, finding a good predictor for martensitic transformation temperature $T_M$ is important. The electron-atom ratio ($e/a$) has been identified to be a predictor of $T_M$ for systems undergoing martensitic transformations: A larger $e/a$ indicates a higher $T_M$ [30–32]. However, such a connection is coarse grained and fails in some situations. For the same $e/a$ ratio, changes in atomic order (site occupancy) also can change the $T_M$. For example, replacement of Ga by Al or In and variations in the long-range atomic order changed $T_M$ without altering the $e/a$ ratio [33–36]. This is also true for Ni-Mn-Sb alloys. Although $T_M$ varies as $e/a$ for $Ni_2Mn_{1+x}Sb_{1-x}$ [24] and for $Ni_{2-x}Mn_{1.56+x}Sb_{0.44}$ [23], Khan *et al.* [37] concluded from their experiments on $Ni_{2+x}Mn_{1.52-x}Sb_{0.48}$ that rather than the $e/a$, it is the hybridization between Ni and excess Mn $3d$ states, which is responsible for variations in the $T_M$. On the other hand, for some alloys undergoing MPT, $T_M$ is found to be closely related to elastic shear modulus C′: the lower the elastic constant, the higher the $T_M$ will be [38,39]. Various off-stoichiometric $Ni_2MnGa$ alloys also show this $T_M$ dependence on C′ [26,40]. The total energy difference $\Delta E$ between the high-temperature parent austenite phase and the low-temperature tetragonal martensite phase is another quantity to correlate with $T_M$ and C′ with the composition of the alloys. A higher $\Delta E$ corresponds to a higher $T_M$ [41,42]. It is therefore of fundamental interest to correlate the trend of variation in $T_M$ for off-stoichiometric Ni-Mn-Sb compositions with these physical quantities and to decide the best predictor of $T_M$ for the considered alloys.

In this paper, we report a systematic study over the entire composition range in Mn and Ni-excess off-stoichiometric $Ni_2MnSb$ systems to explore the importance of various physical factors affecting the phase stability. To this end, we have systematically explored the importance of composition, atomic ordering, and magnetic structure, and the consequences on phase stability and various properties. The microscopic origin of the observed features has been interpreted from the composition, site-ordering, and magnetic-ordering-dependent electronic structures. We have tried to address the reasons behind choice of Sb-deficient systems in experiments, how critical the role of relative compositions of Ni and Mn are in effecting martensitic transformation, how site occupancy and magnetic structure are intricately related with one another to impact the phase stability, and also provided a predictor for martensitic transformation temperature, one that is independent of the details of the off-stoichiometry.

## II. COMPUTATIONAL METHODS

In the present paper, electronic structure calculations were done with spin-polarized density-functional-theory-based projector augmented wave (PAW) method as implemented in Vienna *Ab initio* Simulation Package (VASP) [43–45]. The valence electronic configurations used for the Ni, Mn, and Sb PAW pseudopotentials are $3d^8 4s^2$, $3d^6 4s$, and $5s^2 5p^3$, respectively. For all calculations, we have used the Perdew-Burke-Ernzerhof implementation of generalized gradient approximation for exchange-correlation functional [46]. An energy cut off of 550 eV and a Monkhorst-Pack $11\times11\times11$ $k$-mesh was used for self-consistent calculations. A larger $k$-mesh of $15\times15\times15$ was used for the density of states calculations of all the structures. The convergence criteria for the total energies and the forces on individual atoms were set to $10^{-6}$ eV and $10^{-2}$ eV/Å, respectively, for all calculations.

The elastic constants for the compounds are calculated using energy-strain method only for high-temperature cubic austenite phases. To determine the bulk modulus (B), the total energy vs volume data is fitted to Murnaghan's equation [47]. Then the elastic moduli C′ and $C_{44}$ are calculated [48,49] by considering volume-conserving orthorhombic ($\epsilon_o$) and monoclinic ($\epsilon_m$) deformations of the cubic cell, respectively. Six strains $\epsilon = 0$, 0.01, 0.02, 0.03, 0.04, 0.05 were used to calculate the total energies $E(\epsilon_o)$ and $E(\epsilon_m)$. The elastic moduli (C′ and $C_{44}$) are then obtained by fitting the variation of total energies with distortions to a third-order polynomial equation [49]. $C_{11}$ and $C_{12}$ are then calculated using the relations $B = \frac{1}{3}(C_{11} + 2C_{12})$ and $C' = \frac{1}{2}(C_{11} - C_{12})$.

The isotropic shear modulus, G, is typically calculated as an average of $G_v$, according to the formalism of Voigt [50] and $G_R$, according to the formalism by Reuss [51]. However, in cases of a number of ferromagnetic Heusler alloys, it was found out that $G_v$ using Voigt formalism is closer to the experimental results [27,52]. Hence, we have approximated G as $G_v$ and calculated its value using the relation: $G_v = \frac{1}{5}(C_{11} - C_{12} + 3C_{44})$. Finally, Cauchy pressure ($C^p$) has been calculated as $C^p = (C_{12} - C_{44})$.

## III. RESULTS AND DISCUSSIONS

At high temperature, $Ni_2MnSb$ crystallizes in a $Cu_2MnAl$-type structure, i.e., the regular Heusler $L2_1$ cubic structure belonging to space group no. 225 ($Fm\bar{3}m$) [23,25,53] with three inequivalent Wyckoff positions (4a, 4b, 8c). The Sb atoms and Mn atoms occupy 4a (0, 0, 0) and 4b (0.50, 0.50, 0.50) Wyckoff positions, respectively, and Ni atoms occupy the 8c [(0.25, 0.25, 0.25) and (0.75, 0.75, 0.75)] sites. In the present paper, we have focused on understanding the physics related to MPT and the trend in associated

properties with compositional changes considering four off-stoichiometric $Ni_2MnSb$ systems: (1) $Ni_2Mn_{1+x}Sb_{1-x}$ (sys1), (2) $Ni_{2-x}Mn_{1+x}Sb$ (sys2), (3) $Ni_{2+x}Mn_{1-x}Sb$ (sys3), and (4) $Ni_{2+x}MnSb_{1-x}$ (sys4). The modeling with any arbitrary composition within the formalism employed requires a large supercell and hence is computationally demanding. Hence, we have considered compositions with $x = 0, 0.25, 0.50$, and 0.75. To model the chemical substitution we have taken a 16-atom conventional cubic cell. Thus, chemical substitution of 25%, 50%, and 75% can be modeled by successive replacement of the atoms of one of the constituents. For example, to make a 25% Mn-excess $Ni_2Mn_{1.25}Sb_{0.75}$ composition, one Sb atom out of the four in the conventional cell is to be replaced with one Mn atom. Such a modeling strategy has worked for many other substituted systems in the Heusler family [29,54,55].

### A. Site preference and magnetic ground state

Site occupancy of different atoms for a fixed composition of a system has great importance in deciding the physical properties. Sánchez-Alarcos *et al.* [36] showed that quenching temperature and the subsequent heat treatment change the degree of the $L2_1$ long-range atomic order, i.e., the site occupancy of the alloy and this is a very important issue affecting the martensitic transformation temperature $T_M$ in $Ni_2MnGa$-based alloys. Hence, before proceeding with the investigation on the phase stability and other physical properties, the preferred site-occupation patterns are decided for all systems considered.

For each of the four systems and compositions considered, possible configurations due to different site occupancy and magnetic structures are listed in Tables I and II. Taking the Mn excess at the Sb site $Ni_2Mn_{1+x}Sb_{1-x}$ (sys1) system as an example, for $x = 0.25$, there exist two different site-occupation configurations: (i) the normal site occupation [Fig. 1(b)] where 25% of excess Mn atoms occupy the deficient Sb sub-lattice and (ii) the abnormal site occupation [Fig. 1(c)] where 25% of excess Mn atoms occupy the Ni sublattice and, consequently, the Ni atoms occupy the deficient Sb sublattice. For $x = 0.50$ and $x = 0.75$, the same way—there are three and four different possible site-occupation configurations, respectively. For all cases, configuration S-a is the normal site-occupation configuration. For all compositions, the following nomenclature has been followed: If there are two types of a particular atom, say X, present, then X atom at its original site is denoted as X1, whereas it is denoted as X2 at other than its own site. If there are three types of a particular atom X present, then X1 is the atom at its own site, X2 is the atom at the site originally for any other constituent but the constituent has deficiency in its composition with respect to $Ni_2MnSb$, X3 is the atom at a site other than these two.

The preferred site-occupancy and the corresponding ground state magnetic configuration for a particular system and composition is determined by comparing the electronic energies ($E_0$) and the free energies ($F$) of the configurations considered. The stable site-occupancy is determined by the relative free energy $\Delta F$; the reference being the energy of the configuration with normal site occupancy and the magnetic structure corresponding to that which produces the lowest energy $E_0$. The relative free energy is determined as

$$\Delta F = \Delta E_0 - T\Delta S.$$

The entropy $S$ includes contributions from chemical mixing, lattice vibrations, and magnetic excitations:

$$S = S_{\text{mix}} + S_{\text{vib}} + S_{\text{mag}}.$$

The chemical mixing entropy for a given configuration is determined as

$$S_{\text{mix}} = -\frac{1}{4}k_B \sum_{i=1}^{n}\sum_{j=1}^{4} x_{ij} ln x_{ij},$$

where $x_{ij}$ is the concentration of $i$th component at $j$th sublattice, $n$ is the number of components at corresponding sublattices, $k_B$ is the Boltzmann constant. The entropy difference between configurations due to lattice vibrations is approximated by the high-temperature expansion and given as [56]

$$\Delta S_{\text{vib}} \sim 3k_B(\Delta\Theta/\Theta).$$

In the simplest approximation, the Debye temperatures $\Theta$ are proportional to $\sqrt{rB}$ [57], where $r$ is the Wigner-Seitz radius

TABLE I. Relative electronic energy $\Delta E_0$ (in meV/atom) and relative mixing entropy $\Delta S_{\text{mix}}$ (in meV/K per atom) considering the electronic energy and the mixing entropy of the normal site-occupation configuration with lowest energy magnetic configuration as reference for Mn-excess systems in their $L2_1$ phases: $Ni_2Mn_{1+x}Sb_{1-x}$ (sys1) and $Ni_{2-x}Mn_{1+x}Sb$ (sys2) with $x = 0.25, 0.50$ and 0.75. S-a to S-d and C1 to C4 denote possible site-occupation configurations and possible magnetic configurations, respectively. Boldface indicates the most stable configuration for the corresponding composition.

(i) $Ni_2Mn_{1+x}Sb_{1-x}$ (sys1)

| | | Site Occupancy | | | | | | |
|---|---|---|---|---|---|---|---|---|
| Composition | Site Config. | 4a site | 4b site | 8c site | Magnetic Config. | Name | $\Delta E_0$ | $\Delta S_{\text{mix}}$ |
| $x = 0.25$ | **S-a** | **$Sb1_{0.75}Mn2_{0.25}$** | **Mn1** | **$Ni1_2$** | **C1 (Ni1↑ Mn1↑ Mn2↓)** | **S-a-C1** | 0.00 | 0.00 |
| **$Ni_2Mn_{1.25}Sb_{0.75}$** | | | | | C2 (Ni1↑ Mn1↑ Mn2↑) | S-a-C2 | 11.70 | 0.00 |
| | S-b | $Sb1_{0.75}Ni2_{0.25}$ | Mn1 | $Ni1_{1.75}Mn2_{0.25}$ | C1 (Ni1↑ Ni2↑ Mn1↑ Mn2↓) | S-b-C1 | 33.61 | 0.00812 |
| | | | | | C2 (Ni1↑ Ni2↑ Mn1↑ Mn2↑) | S-b-C2 | 55.51 | 0.00825 |

TABLE I. (*Continued*).

(i) $Ni_2Mn_{1+x}Sb_{1-x}$ (sys1)

| Composition | Site Config. | Site Occupancy 4a site | 4b site | 8c site | Magnetic Config. | Name | $\Delta E_0$ | $\Delta S_{mix}$ |
|---|---|---|---|---|---|---|---|---|
| $x = 0.50$ | **S-a** | **$Sb1_{0.50}Mn2_{0.50}$** | **Mn1** | **$Ni1_2$** | **C1 (Ni1↑ Mn1↑ Mn2↓)** | **S-a-C1** | 0.00 | 0.00 |
| **$Ni_2Mn_{1.50}Sb_{0.50}$** | | | | | C2 (Ni1↑ Mn1↑ Mn2↑) | S-a-C2 | 15.32 | 0.00 |
| | S-b | $Sb1_{0.50}Ni2_{0.50}$ | Mn1 | $Ni1_{1.50}Mn2_{0.50}$ | C1 (Ni1↑ Ni2↑ Mn1↑ Mn2↓) | S-b-C1 | 38.58 | 0.0242 |
| | | | | | C2 (Ni1↑ Ni2↑ Mn1↑ Mn2↑) | S-b-C2 | 90.36 | 0.0242 |
| | S-c | $Sb1_{0.50}Mn2_{0.25}Ni2_{0.25}$ | Mn1 | $Ni1_{1.75}Mn3_{0.25}$ | C1 (Ni1↑ Ni2↑ Mn1↑ Mn2↓ Mn3↓) | S-c-C1 | 30.98 | 0.0237 |
| | | | | | C2 (Ni1↑ Ni2↑ Mn1↑ Mn2↑ Mn3↑) | S-c-C2 | 55.36 | 0.0237 |
| | | | | | C3 (Ni1↑ Ni2↑ Mn1↑ Mn2↓ Mn3↑) | S-c-C3 | 44.67 | 0.0237 |
| | | | | | C4 (Ni1↑ Ni2↑ Mn1↑ Mn2↑ Mn3↓) | S-c-C4 | 36.86 | 0.0237 |
| $x = 0.75$ | **S-a** | **$Sb1_{0.25}Mn2_{0.75}$** | **Mn1** | **$Ni1_2$** | **C1 (Ni1↑ Mn1↑ Mn2↓)** | **S-a-C1** | 0.00 | 0.00 |
| **$Ni_2Mn_{1.75}Sb_{0.25}$** | | | | | C2 (Ni1↑ Mn1↑ Mn2↑) | S-a-C2 | 15.02 | 0.00 |
| | S-b | $Sb1_{0.25}Ni2_{0.75}$ | Mn1 | $Ni1_{1.25}Mn2_{0.75}$ | C1 (Ni1↑ Ni2↑ Mn1↑ Mn2↓) | S-b-C1 | 35.40 | 0.0285 |
| | | | | | C2 (Ni1↑ Ni2↑ Mn1↑ Mn2↑) | S-b-C2 | 139.32 | 0.0285 |
| | S-c | $Sb1_{0.25}Mn2_{0.25}Ni2_{0.50}$ | Mn1 | $Ni1_{1.50}Mn3_{0.50}$ | C1 (Ni1↑ Ni2↑ Mn1↑ Mn2↓ Mn3↓) | S-c-C1 | 50.35 | 0.0345 |
| | | | | | C2 (Ni1↑ Ni2↑ Mn1↑ Mn2↑ Mn3↑) | S-c-C2 | 124.78 | 0.0345 |
| | | | | | C3 (Ni1↑ Ni2↑ Mn1↑ Mn2↓ Mn3↑) | S-c-C3 | 85.97 | 0.0345 |
| | | | | | C4 (Ni1↑ Ni2↑ Mn1↑ Mn2↑ Mn3↓) | S-c-C4 | 44.10 | 0.0345 |
| | S-d | $Sb1_{0.25}Mn2_{0.50}Ni2_{0.25}$ | Mn1 | $Ni1_{1.75}Mn3_{0.25}$ | C1 (Ni1↑ Ni2↑ Mn1↑ Mn2↓ Mn3↓) | S-d-C1 | 36.27 | 0.0265 |
| | | | | | C2 (Ni1↑ Ni2↑ Mn1↑ Mn2↑ Mn3↑) | S-d-C2 | 74.86 | 0.0265 |
| | | | | | C3 (Ni1↑ Ni2↑ Mn1↑ Mn2↓ Mn3↑) | S-d-C3 | 45.42 | 0.0265 |
| | | | | | C4 (Ni1↑ Ni2↑ Mn1↑ Mn2↑ Mn3↓) | S-d-C4 | 35.72 | 0.0265 |

(ii) $Ni_{2-x}Mn_{1+x}Sb$ (sys2)

| Composition | Site Config. | Site Occupancy 4a site | 4b site | 8c site | Magnetic Config. | Name | $\Delta E_0$ | $\Delta S_{mix}$ |
|---|---|---|---|---|---|---|---|---|
| $x = 0.25$ | **S-a** | **Sb1** | **Mn1** | **$Ni1_{1.75}Mn2_{0.25}$** | **C1 (Ni1↑ Mn1↑ Mn2↓)** | **S-a-C1** | 0.00 | 0.00 |
| **$Ni_{1.75}Mn_{1.25}Sb$** | | | | | C2 (Ni1↑ Mn1↑ Mn2↑) | S-a-C2 | 7.52 | 0.00 |
| | S-b | $Sb1_{0.75}Mn2_{0.25}$ | Mn1 | $Ni1_{1.75}Sb2_{0.25}$ | C1 (Ni1↑ Ni2↑ Mn1↑ Mn2↓) | S-b-C1 | 98.41 | 0.0121 |
| | | | | | C2 (Ni1↑ Ni2↑ Mn1↑ Mn2↑) | S-b-C2 | 128.76 | 0.0121 |
| $x = 0.50$ | **S-a** | **Sb1** | **Mn1** | **$Ni1_{1.50}Mn2_{0.50}$** | **C1 (Ni1↑ Mn1↑ Mn2↓)** | **S-a-C1** | 0.00 | 0.00 |
| **$Ni_{1.50}Mn_{1.50}Sb$** | | | | | C2 (Ni1↑ Mn1↑ Mn2↑) | S-a-C2 | 20.75 | 0.00 |
| | S-b | $Sb1_{0.50}Mn2_{0.50}$ | Mn1 | $Ni1_{1.50}Sb2_{0.50}$ | C1 (Ni1↑ Mn1↑ Mn2↓) | S-b-C1 | 110.85 | 0.0149 |
| | | | | | C2 (Ni1↑ Mn1↑ Mn2↑) | S-b-C2 | 141.96 | 0.0149 |
| | S-c | $Sb1_{0.75}Mn3_{0.25}$ | Mn1 | $Ni1_{1.50}Mn2_{0.25}Sb2_{0.25}$ | C1 (Ni1↑ Mn1↑ Mn2↓ Mn3↓) | S-c-C1 | 95.09 | 0.0195 |
| | | | | | C2 (Ni1↑ Mn1↑ Mn2↑ Mn3↑) | S-c-C2 | 137.95 | 0.0195 |
| | | | | | C3 (Ni1↑ Mn1↑ Mn2↑ Mn3↓) | S-c-C3 | 108.98 | 0.0195 |
| | | | | | C4 (Ni1↑ Mn1↑ Mn2↓ Mn3↑) | S-c-C4 | 119.32 | 0.0195 |
| $x = 0.75$ | **S-a** | **Sb1** | **Mn1** | **$Ni1_{1.25}Mn2_{0.75}$** | **C1 (Ni1↑ Mn1↑ Mn2↓)** | **S-a-C1** | 0.00 | 0.00 |
| **$Ni_{1.25}Mn_{1.75}Sb$** | | | | | C2 (Ni1↑ Mn1↑ Mn2↑) | S-a-C2 | 36.12 | 0.00 |
| | S-b | $Sb1_{0.25}Mn2_{0.75}$ | Mn1 | $Ni1_{1.25}Sb2_{0.75}$ | C1 (Ni1↑ Mn1↑ Mn2↓) | S-b-C1 | 93.44 | 0.0121 |
| | | | | | C2 (Ni1↑ Mn1↑ Mn2↑) | S-b-C2 | 161.2 | 0.0121 |
| | S-c | $Sb1_{0.50}Mn3_{0.50}$ | Mn1 | $Ni1_{1.25}Mn2_{0.25}Sb2_{0.50}$ | C1 (Ni1↑ Mn1↑ Mn2↓ Mn3↓) | S-c-C1 | 106.33 | 0.0252 |
| | | | | | C2 (Ni1↑ Mn1↑ Mn2↑ Mn3↑) | S-c-C2 | 161.19 | 0.0252 |
| | | | | | C3 (Ni1↑ Mn1↑ Mn2↑ Mn3↓) | S-c-C3 | 116.57 | 0.0252 |
| | | | | | C4 (Ni1↑ Mn1↑ Mn2↓ Mn3↑) | S-c-C4 | 127.57 | 0.0252 |
| | S-d | $Sb1_{0.75}Mn3_{0.25}$ | Mn1 | $Ni1_{1.25}Mn2_{0.50}Sb2_{0.25}$ | C1 (Ni1↑ Mn1↑ Mn2↓ Mn3↓) | S-d-C1 | 87.43 | 0.0224 |
| | | | | | C2 (Ni1↑ Mn1↑ Mn2↑ Mn3↑) | S-d-C2 | 149.99 | 0.0224 |
| | | | | | C3 (Ni1↑ Mn1↑ Mn2↑ Mn3↓) | S-d-C3 | 124.21 | 0.0224 |
| | | | | | C4 (Ni1↑ Mn1↑ Mn2↓ Mn3↑) | S-d-C4 | 106.82 | 0.0224 |

TABLE II. Relative electronic energy $\Delta E_0$ (in meV/atom) and relative mixing entropy $\Delta S_{mix}$ (in meV/K per atom), considering the electronic energy and the mixing entropy of the normal site-occupation configuration with lowest energy magnetic configuration as reference for Ni-excess systems in their $L2_1$ phases: $Ni_{2+x}Mn_{1-x}Sb$ (sys3) and $Ni_{2+x}MnSb_{1-x}$ (sys4) with $x = 0.25$, 0.50 and 0.75. S-a to S-d and C1 to C4 denote possible site-occupation configurations and corresponding magnetic configurations, respectively. Boldface indicates the most stable configuration for the corresponding composition.

(iii) $Ni_{2+x}Mn_{1-x}Sb$ (sys3)

| | | Site Occupancy | | | | | | |
|---|---|---|---|---|---|---|---|---|
| Composition | Site Config. | 4a site | 4b site | 8c site | Magnetic Config. | Name | $\Delta E_0$ | $\Delta S_{mix}$ |
| $x = 0.25$ **$Ni_{2.25}Mn_{0.75}Sb$** | **S-a** | **Sb1** | **$Mn1_{0.75}Ni2_{0.25}$** | **$Ni1_2$** | **C2 (Ni1↑ Ni2↑ Mn1↑)** | **S-a-C2** | 0.00 | 0.00 |
| | S-b | $Sb1_{0.75}Ni2_{0.25}$ | $Mn1_{0.75}Sb2_{0.25}$ | $Ni1_2$ | C2 (Ni1↑ Ni2↑ Mn1↑) | S-b-C2 | 140.28 | 0.0123 |
| $x = 0.50$ **$Ni_{2.50}Mn_{0.50}Sb$** | **S-a** | **Sb1** | **$Mn1_{0.50}Ni2_{0.50}$** | **$Ni1_2$** | **C2 (Ni1↑ Ni2↑ Mn1↑)** | **S-a-C2** | 0.00 | 0.00 |
| | S-b | $Sb1_{0.50}Ni2_{0.50}$ | $Mn1_{0.50}Sb2_{0.50}$ | $Ni1_2$ | C2 (Ni1↑ Ni2↑ Mn1↑) | S-b-C2 | 170.75 | 0.015 |
| | S-c | $Sb1_{0.75}Ni3_{0.25}$ | $Mn1_{0.50}Ni2_{0.25}Sb2_{0.25}$ | $Ni1_2$ | C2 (Ni1↑ Ni2↑ Ni3↑ Mn1↑) | S-c-C2 | 164.36 | 0.0194 |
| $x = 0.75$ **$Ni_{2.75}Mn_{0.25}Sb$** | **S-a** | **Sb1** | **$Mn1_{0.25}Ni2_{0.75}$** | **$Ni1_2$** | **C2 (Ni1↑ Ni2↑ Mn1↑)** | **S-a-C2** | 0.00 | 0.00 |
| | S-b | $Sb1_{0.25}Ni2_{0.75}$ | $Mn1_{0.25}Sb2_{0.75}$ | $Ni1_2$ | C2 (Ni1↑ Ni2↑ Mn1↑) | S-b-C2 | 148.74 | 0.0121 |
| | S-c | $Sb1_{0.50}Ni3_{0.50}$ | $Mn1_{0.25}Ni2_{0.25}Sb2_{0.50}$ | $Ni1_2$ | C2 (Ni1↑ Ni2↑ Ni3↑ Mn1↑) | S-c-C2 | 204.67 | 0.0252 |
| | S-d | $Sb1_{0.75}Ni3_{0.25}$ | $Mn1_{0.25}Ni2_{0.50}Sb2_{0.25}$ | $Ni1_2$ | C2 (Ni1↑ Ni2↑ Ni3↑ Mn1↑) | S-d-C2 | 170.92 | 0.0224 |

(iv) $Ni_{2+x}MnSb_{1-x}$ (sys4)

| | | Site Occupancy | | | | | | |
|---|---|---|---|---|---|---|---|---|
| Composition | Site Config. | 4a site | 4b site | 8c site | Magnetic Config. | Name | $\Delta E_0$ | $\Delta S_{mix}$ |
| $x = 0.25$ **$Ni_{2.25}MnSb_{0.75}$** | S-a | $Sb1_{0.75}Ni2_{0.25}$ | Mn1 | $Ni1_2$ | C2 (Ni1↑ Ni2↑ Mn1↑) | S-a-C2 | 0.00 | 0.00 |
| | **S-b** | **$Sb1_{0.75}Mn2_{0.25}$** | **$Mn1_{0.75}Ni2_{0.25}$** | **$Ni1_2$** | **C1 (Ni1↑ Ni2↑ Mn1↑ Mn2↓)** | **S-b-C1** | −15.78 | 0.012 |
| | | | | | C2 (Ni1↑ Ni2↑ Mn1↑ Mn2↑) | S-b-C2 | −6.94 | 0.0123 |
| $x = 0.50$ **$Ni_{2.50}MnSb_{0.50}$** | S-a | $Sb1_{0.50}Ni2_{0.50}$ | Mn1 | $Ni1_2$ | C2 (Ni1↑ Ni2↑ Mn1↑) | S-a-C2 | 0.00 | 0.00 |
| | **S-b** | **$Sb1_{0.50}Mn2_{0.50}$** | **$Mn1_{0.50}Ni2_{0.50}$** | **$Ni1_2$** | **C1 (Ni1↑ Ni2↑ Mn1↑ Mn2↓)** | **S-b-C1** | −9.75 | 0.0149 |
| | | | | | C2 (Ni1↑ Ni2↑ Mn1↑ Mn2↑) | S-b-C2 | 4.14 | 0.0149 |
| | **S-c** | **$Sb1_{0.50}Mn2_{0.25}Ni2_{0.25}$** | **$Mn1_{0.75}Ni3_{0.25}$** | **$Ni1_2$** | **C1 (Ni1↑ Ni2↑ Ni3↑ Mn1↑ Mn2↓)** | **S-c-C1** | −9.78 | 0.0195 |
| | | | | | C2 (Ni1↑ Ni2↑ Ni3↑ Mn1↑ Mn2↑) | S-c-C2 | −2.67 | 0.0195 |
| $x = 0.75$ **$Ni_{2.75}MnSb_{0.25}$** | S-a | $Sb1_{0.25}Ni2_{0.75}$ | Mn1 | $Ni1_2$ | C2 (Ni1↑ Ni2↑ Mn1↑) | S-a-C2 | 0.00 | 0.00 |
| | **S-b** | **$Sb1_{0.25}Mn2_{0.75}$** | **$Mn1_{0.25}Ni2_{0.75}$** | **$Ni1_2$** | **C1 (Ni1↑ Ni2↑ Mn1↓ Mn2↑)** | **S-b-C1** | −6.72 | 0.0121 |
| | | | | | C2 (Ni1↑ Ni2↑ Mn1↑ Mn2↑) | S-b-C2 | 2.23 | 0.0121 |
| | S-c | $Sb1_{0.25}Mn2_{0.50}Ni2_{0.25}$ | $Mn1_{0.50}Ni3_{0.50}$ | $Ni1_2$ | C1 (Ni1↑ Ni2↑ Ni3↑ Mn1↑ Mn2↓) | S-c-C1 | −1.88 | 0.0252 |
| | | | | | C2 (Ni1↑ Ni2↑ Ni3↑ Mn1↑ Mn2↑) | S-c-C2 | 0.73 | 0.0252 |
| | S-d | $Sb1_{0.25}Mn2_{0.25}Ni2_{0.50}$ | $Mn1_{0.75}Ni3_{0.25}$ | $Ni1_2$ | C1 (Ni1↑ Ni2↑ Ni3↑ Mn1↑ Mn2↓) | S-d-C1 | 2.39 | 0.0224 |
| | | | | | C2 (Ni1↑ Ni2↑ Ni3↑ Mn1↑ Mn2↑) | S-d-C2 | 0.78 | 0.0224 |

and $B$ is the bulk modulus. The contributions of the magnetic excitations to the entropy is calculated invoking the disordered local moment [58] to approximate the fully spin disordered phase. In the mean-field approximation, the entropy due to magnetic disorder is given as [59]

$$S_{mag} = k_B \sum_i ln(\mu_i + 1).$$

$\mu_i$ is the magnetic moment of the $i$th component. Our results for $\Delta S_{mix}$ and $\Delta S_{vib}$ are given in Table I of Ref. [60]. In all cases, the contribution of $\Delta S_{vib}$ is atleast 1 to 2 orders of magnitude smaller than that of $\Delta S_{mix}$. Similarly, $\Delta S_{mag}$ is at most of the order of $\Delta S_{vib}$ in some cases (for example, $\Delta S_{mag}$ for S-b-C1 configuration of sys1 with $x = 0.25$ is only 0.00367 meV/K) even after consideration of the fully spin-disordered phase. Therefore, the contributions from lattice vibrations

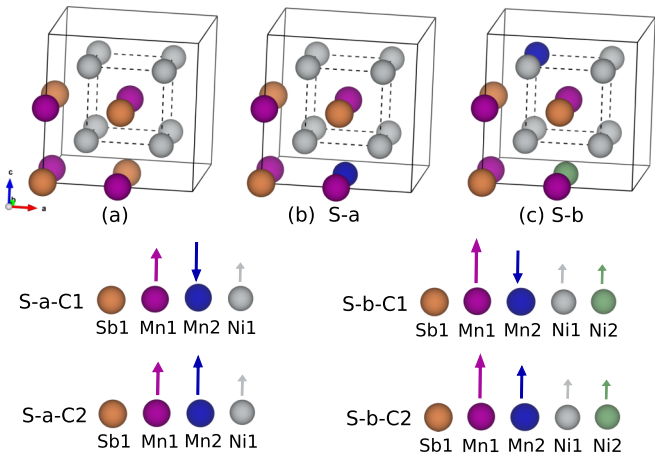


FIG. 1. Sixteen-atom supercells for (a) stoichiometric $Ni_2MnSb$ and (b)–(c) off-stoichiometric $Ni_2Mn_{1+x}Sb_{1-x}$ (sys1) with $x = 0.25$ for (b) normal site-occupation configuration (S-a) and (c) abnormal site-occupation configuration (S-b), respectively. S-a-C1, S-a-C2 indicate the possible different magnetic configurations corresponding to S-a site configuration and S-b-C1, S-b-C2 indicate the same corresponding to S-b. Different types of atoms have been referred to by their corresponding color. The arrows indicate the spin orientations of the atoms with respect to $z$ axis. An up arrow indicates positive $z$ direction or spin up. The magnetic configurations C1 and C2 are explained in Table I.

and magnetic excitations are neglected in total $\Delta S$ as at the ambient condition of $T = 300$ K and at typical annealing temperature of the order of 1000 K, their contributions are not significant enough toward $\Delta F$. In what follows, in Tables I and II, alongside $\Delta E_0$, the relative energy with respect to the minimum total energy, we present only the values of $\Delta S_{\text{mix}}$. It can be noted that even at the typical annealing temperature of the order of 1000 K, the $\Delta F$ comprising contributions of only mixing entropy will have the same trend as $\Delta E_0$. Therefore, in the temperature range of interest, the mixing entropy cannot change the relative stability of the different site occupations and magnetic configurations. Thus, consideration of the relative electronic energy ($\Delta E_0$) is sufficient to determine the preferred site and the magnetic configuration.

From Table I, it can be seen that for all compositions in Mn-excess off-stoichiometric systems (i.e., sys1 and sys2), the normal site occupation (i.e.,S-a), where excess Mn atoms occupy the deficient atom sublattice, is preferred over abnormal ones, and for all preferred site-occupation configurations, magnetic configuration C1 is the ground state in which the Mn atom at its original sublattice (denoted as Mn1) and the Mn atom at the deficient atom sublattice (denoted as Mn2) align antiparallel. Previous experimental and theoretical investigations [61,62] also showed a ferrimagnetic coupling between the Mn1 and Mn2 atoms in Sb-deficient Mn-excess Ni-Mn-Sb compositions. For Ni-excess systems, as has been shown in Table II, depending upon the deficiency of Mn or Sb in the systems, preferred site occupancy can be normal or abnormal. For the Mn-deficient system (sys3), normal site-occupation configuration (S-a) with C2 magnetic structure is stable for all the compositions. For the Sb-deficient system (sys4), it is the abnormal one which has the lowest energy for each of the compositions. In this system, for both 25% and 75% substitutions S-b-C1, where the excess Ni atoms prefer the Mn sublattice although the compositions have Sb deficiency, is the lowest energy configuration whereas, for $x = 0.50$, almost the same energy for S-b-C1 and S-c-C1 suggests that these configurations may coexist in the alloy.

### B. Structural parameters and magnetic moments

The equilibrium lattice constants for the minimum energy configurations for each system and composition in the $L2_1$ phases are listed in Table III. The variations in the lattice

TABLE III. Calculated values of electron to atom ratio ($e/a$), equilibrium lattice constant ($a_0$), total magnetic moment ($M_A$) of the four Ni-Mn-Sb systems in their $L2_1$ phases. The total energy difference ($\Delta E$) between the austenite ($L2_1$) and the martensite (tetragonal) phases (the equilibrium value of tetragonal distortion (c/a) is given in parentheses), the corresponding volume change($|\Delta V|/V$) with respect to $L2_1$ structure are given. Reported values of lattice constants in the literature are also given.

| Composition | Configuration | e/a | $a_0$(Å) | $\Delta E(c/a)$ (meV/atom) | $\lvert\Delta V\rvert/V$ (%) | $M_A$ ($\mu_B/f.u.$) | $a_0^{\text{Lit.}}$(Å) |
|---|---|---|---|---|---|---|---|
| $Ni_2MnSb$ | S-a-C2 | 8.00 | 6.06 | – | – | 3.99 | 6.027 [25], 6.0031 [24] |
| $Ni_2Mn_{1.25}Sb_{0.75}$ | S-a-C1 | 8.125 | 6.00 | 2.56(1.28) | 0.54 | 2.86 | 6.018 [25] ($x = 0.24$) |
| $Ni_2Mn_{1.50}Sb_{0.50}$ | S-a-C1 | 8.25 | 5.94 | 25.14(1.32) | 1.60 | 1.71 | 5.98 [25], 5.97 [63] |
| $Ni_2Mn_{1.75}Sb_{0.25}$ | S-a-C1 | 8.375 | 5.86 | 55.32(1.36) | 1.69 | 0.69 | – |
| $Ni_{1.75}Mn_{1.25}Sb$ | S-a-C1 | 7.8125 | 6.09 | – | – | 3.27 | – |
| $Ni_{1.50}Mn_{1.50}Sb$ | S-a-C1 | 7.625 | 6.10 | – | – | 2.49 | – |
| $Ni_{1.25}Mn_{1.75}Sb$ | S-a-C1 | 7.4375 | 6.12 | – | – | 1.59 | – |
| $Ni_{2.25}Mn_{0.75}Sb$ | S-a-C2 | 8.1875 | 6.04 | – | – | 2.94 | – |
| $Ni_{2.50}Mn_{0.50}Sb$ | S-a-C2 | 8.375 | 6.01 | – | – | 1.93 | – |
| $Ni_{2.75}Mn_{0.25}Sb$ | S-a-C2 | 8.5625 | 5.98 | – | – | 1.03 | – |
| $Ni_{2.25}MnSb_{0.75}$ | S-b-C1 | 8.3125 | 5.96 | 13.3(1.31) | 0.55 | 1.78 | – |
| $Ni_{2.50}MnSb_{0.50}$ | S-b-C1 | 8.625 | 5.88 | 54.88(1.38) | 1.75 | 0.00 | – |
| | S-c-C1 | 8.625 | 5.88 | 36.46(1.34) | 1.22 | 2.08 | – |
| $Ni_{2.75}MnSb_{0.25}$ | S-b-C1 | 8.9375 | 5.78 | 61.05(1.40) | 2.30 | 2.10 | – |

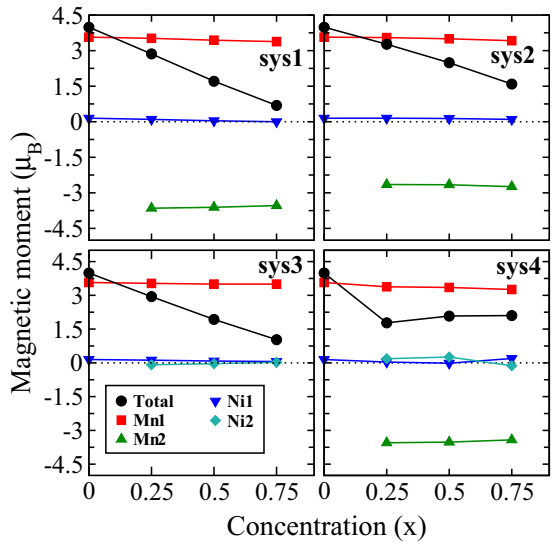


FIG. 2. Calculated total magnetic moment in $\mu_B/f.u.$ and atomic magnetic moments (for atom-name convention, see Sec. IIIA) as a function of concentration of excess atom $x$ for all four systems: $Ni_2Mn_{1+x}Sb_{1-x}$ (sys1), $Ni_{2-x}Mn_{1+x}Sb$ (sys2), $Ni_{2+x}Mn_{1-x}Sb$ (sys3), and $Ni_{2+x}MnSb_{1-x}$ (sys4) in their minimum energy configurations as indicated in Tables I and II.

constants with $x$ for all systems can be understood from the relative sizes of the atomic radii (the atomic radii of Mn, Ni, and Sb are 1.40 Å, 1.35 Å, 1.45 Å, respectively) of the constituents. The trend in the variation of our calculated lattice constants agrees well with the experimental results available for the Mn-excess Sb-deficient system (sys1) [24,25].

In Table III and Fig. 2, we show the variations in the total and atomic magnetic moments in the $L2_1$ phase as a function of composition for each of the four systems considered. For sys1, sys2, and sys3, the total moments decrease with $x$ while for sys4, the variation is nonmonotonic. Also, there is no uniform trend in the variation of the total moment with $(e/a)$. For sys1, the trend agrees well with the experimental observation [25]. Our calculations establish the prediction based upon experimental results [15,25] that the decrease in moment with increase in Mn content is due to antiparallel alignment of Mn1 and Mn2. Same is true for sys2. For Ni-excess, Mn-deficient system (sys3), the same trend is observed, albeit not because of antiparallel alignment of Mn atoms at different sites but because of decrease in the Mn content, the largest contributor to the total magnetic moment. The nonmonotonic trend seen in sys4 can be attributed to the presence of Mn and Ni at two different sites. The trends in the atomic moments suggest that the moment of each constituent element remains nearly constant across systems and compositions. Thus, the trends in the total moment are controlled by concentration alone.

### C. Composition-dependent structural phase stability

As stated in the Introduction, some of the Sb-deficient Ni-Mn-Sb alloys with either or both Ni or Mn content higher than that in the stoichiometric composition of 2:1:1 in $Ni_2MnSb$ exhibit shape-memory and magnetocaloric effects [15,22,23,25,37,64] which are artefacts of $L2_1$ to tetragonal structural transformation (martensitic transformation). After ascertaining the ground-state atomic and magnetic configurations of each of the four systems considered, we now investigate the relative stabilities of the $L2_1$ austenite and the tetragonal martensite phases. This investigation will shed light on the dependence of the stability of the high-temperature austenite phase on the details of composition. We proceed to do this by distorting the $L2_1$ structure along $z$ axis and computing the total energy as a function of the tetragonal distortion, given by $(c/a)$. This is done for the ground-state configuration for each system and each composition. In each case, the composition with $x = 0.50$ required special treatment. Due to the finite size of the 16-atom supercell, two crystallographic inequivalent directions appear in the supercell only for compositions with $x = 0.50$. In this case, the tetragonal distortion can be applied parallel to or perpendicular to the plane defined by the two atoms which are deficient with respect to stoichiometric composition of 2:1:1 (8:4:4 in the 16-atom supercell) for sys1, sys3, and sys4, and by the two atoms which are excess in sys2. Accordingly, the total energies are computed with respect to both distortions and averaged (the two curves corresponding to distortions in two different directions for each case are shown in Fig. 1 of Ref. [60]). The results are presented in Fig. 3.

For sys1, i.e., Mn-excess and Sb-deficient system, it can be seen that the stability of the austenite $L2_1$ phase decreases with the increasing concentration $x$ of the excess Mn atoms at the expense of Sb atoms. The increase of $\Delta E$ (see Table III) with $x$ suggests that as the Sb (Mn) concentration gradually decreases (increases), the martensitic transformation would take place at higher temperature. This trend is in good agreement with the experimental observations [22,23,25] that the martensitic transformation temperature $T_M$ increases with decrease in Sb concentration for $Ni_2Mn_{1+x}Sb_{1-x}$ alloys. For sys2 and sys3, those are the two systems where Sb concentration is that of the stoichiometric $Ni_2MnSb$, the austenite phase is stable throughout the entire composition range considered. In case of sys3, a weak tendency towards destabilization of the austenite phase is observed when $x = 0.75$. For sys4, i.e., Ni-excess and Sb-deficient system, the tetragonal phase is stable for all compositions with $\Delta E$ as large as ~61 meV/atom for $x = 0.75$. Our calculations, thus suggest that the $L2_1$ phase in Ni-Mn-Sb system can be destabilized leading to a martensitic transformation only when Sb content in the system is about 12.5% (25%) or less for Mn-excess (Ni-excess) systems. This also suggests why experiments to observe functional properties driven by martensitic phase transformation were always done at compositions with Sb content around 12.5%.

### D. Dependence of phase stability on site-occupancy and magnetic structure

Site ordering and magnetic structure can affect the possibility of a martensitic transformation in Heusler alloys. Ghosh *et al.* [65] observed that, depending on annealing time, site occupancy in $Ni_2Mn_{1.46}Sn_{0.54}$ can change, affecting the magnetocaloric properties as a consequence. In $Ni_2Mn_{1+x}In_{1-x}$, it was observed that the martensitic phase transformation happens only when the Mn atoms at different sites align antiparallel [28]. In this subsection, we therefore examine

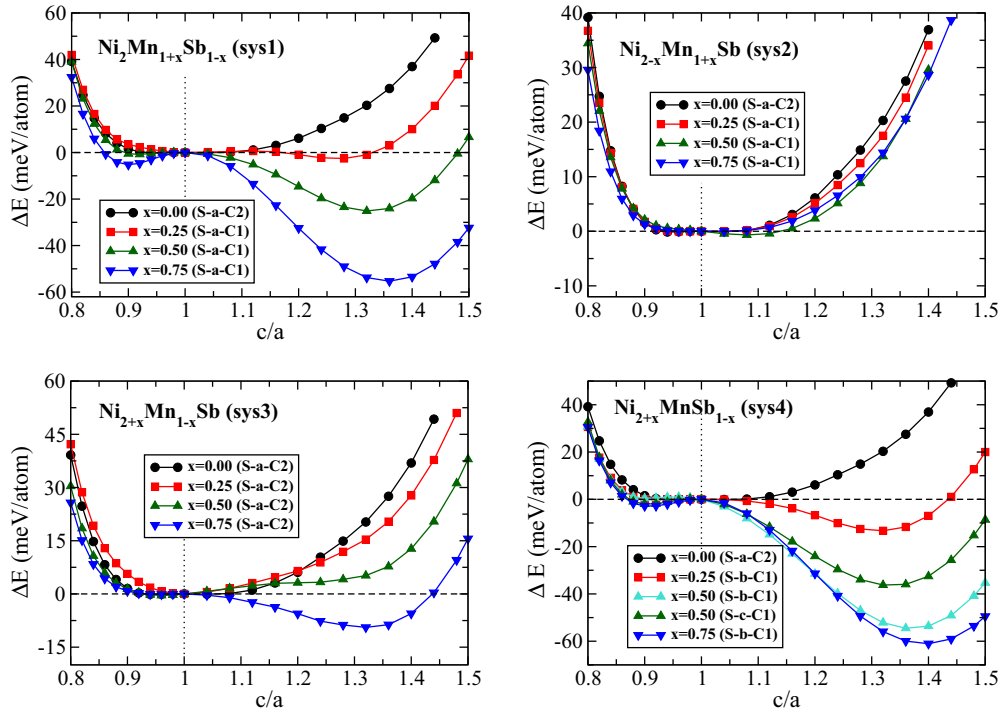


FIG. 3. The variations of total energy difference ($\Delta E$) between the austenite ($L2_1$) and the martensite (tetragonal) phases as a function of tetragonal distortion, i.e., $c/a$ ratio for all four systems with different compositions and at their minimum-energy configurations.

the dependencies of the relative stabilities of the two phases on the site-occupancy configurations and the magnetic structures. We do so by picking up only those configurations corresponding to each of the four systems and compositions which have energies in their $L2_1$ phases lying right above the corresponding ground-state energies and computing their total energy surfaces as a function of tetragonal distortions. In choosing the configurations from Tables I and II following this procedure, we have made exceptions in only two cases: (i) in sys1, for $x = 0.75$, i.e., $Ni_2Mn_{1.75}Sb_{0.25}$ composition, though S-b-C1 has lower energy than S-d-C1, we have chosen S-d-C1 to compare, to maintain the same site-occupancy pattern as that of $x = 0.25$ and 0.50 compositions, and (ii) in sys4, since an abnormal configuration is always the lowest energy one, we have considered the normal configuration for the purpose of comparison even though it is not the one having energy right above the minimum. The configurations picked up are marked by enclosing boxes around them in Tables I and II. For these calculations, optimized lattice constants corresponding to each configuration have been used. The results are presented in Fig. 4.

We divide the systems into two categories: (i) ones with Sb concentration equal to that of $Ni_2MnSb$, but with excess-Mn or excess-Ni (sys2 and sys3, respectively), (ii) Sb-deficient ones, but with excess-Mn or excess-Ni (sys1 and sys4, respectively) for the purpose of discussion. For category (i), the total energy results suggest that an abnormal site occupancy where Mn atoms occupy Sb sites also is the key factor destabilizing the austenite phase, effecting a martensitic transformation. Thus, irrespective of whether site occupancy is normal or abnormal, the austenite phase is nearly stable across compositions in sys3, as in such a Mn-deficient system, Mn can occupy its own site only. In sys2, the abnormal site-occupancy leads to destabilization of the austenite phase across compositions as in abnormal occupancy patterns considered here, extra Mn atoms occupy both Ni and Sb sites. For category (ii), both site ordering and spin alignment of Mn atoms at different sites contribute toward phase stability along with the content of Sb. In sys1, with the highest Sb-content ($Ni_2Mn_{1.25}Sb_{0.75}$), a parallel alignment between Mn atoms at its original site and at the Sb site with normal site configuration produces minimum total energy in the $L2_1$ phase. The stability is disturbed when the alignment is antiparallel, leading to a rather shallow minima for $c/a \neq 1$. With an abnormal site configuration where excess Mn occupies Ni site rather than Sb site, the destabilization of the austenite phase becomes prominent, and the alignment of Mn spins does not matter. As Sb-content decreases, the martensitic phase becomes stable for abnormal site configuration, irrespective of the magnetic structure. However, with normal site configuration, a magnetic structure where Mn moments align parallel stabilize the austenite phase. Thus, the ferromagnetic ordering stabilizes the austenite phase in this system when site-occupancy is normal. The opposite picture is seen in case of sys4, which is Ni excess and Sb deficient. Baring the highest Sb-content compound, the austenite phase is significantly destabilized irrespective of site-occupancy configurations and orientation of Mn spins. Hence, we can conclude that to stabilize the austenite phase and effect a martensitic transformation in the Ni-Mn-Sb family, the requirements are an abnormal site occupancy and the presence of Mn at Sb site apart from its own site, with their moments aligning antiparallel. This means that controlling the site ordering by manipulating the annealing or preparing the sample by no-equilibrium methods

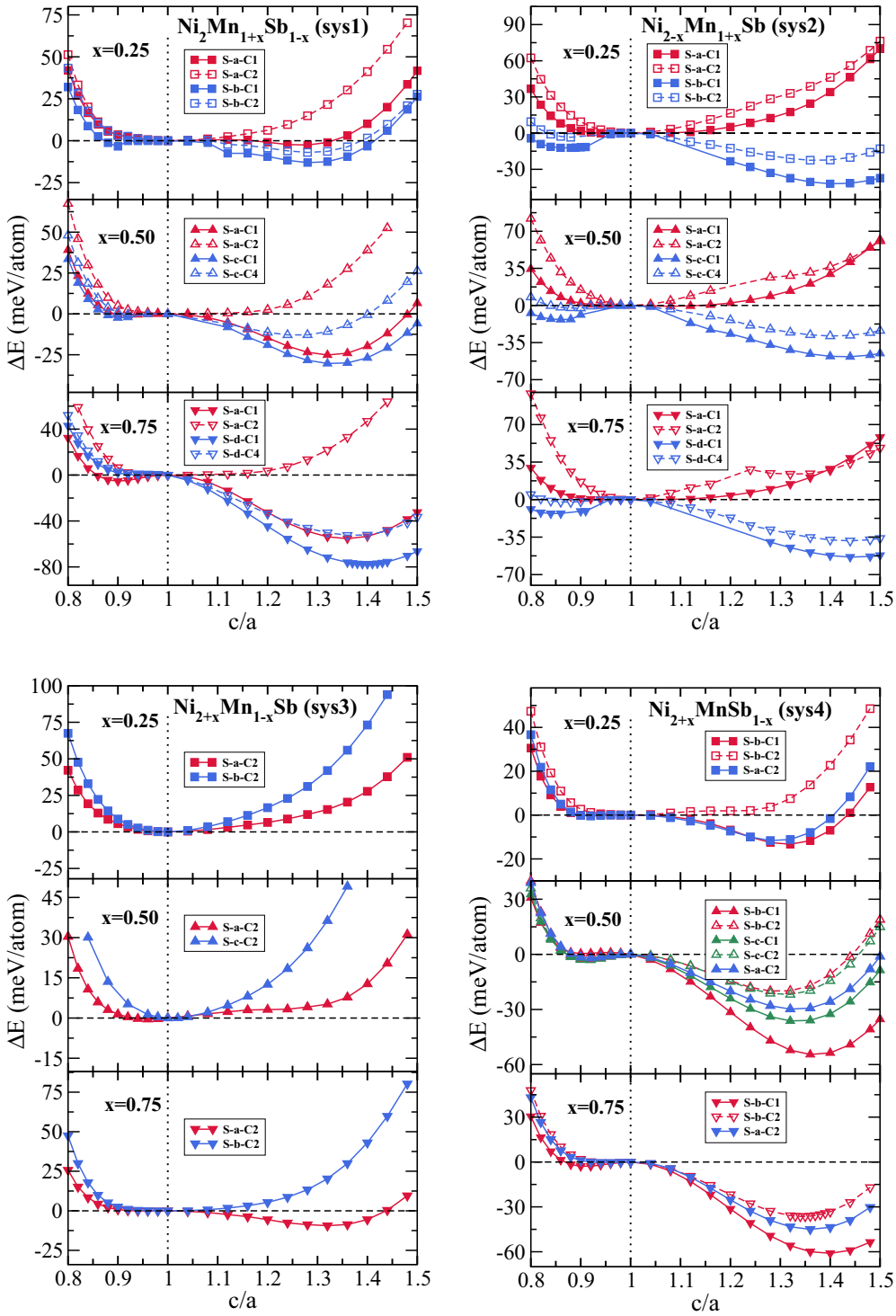


FIG. 4. The variations of total energy difference ($\Delta E$) between the austenite ($L2_1$) and the martensite (tetragonal) phases as a function of tetragonal distortion, i.e., $c/a$ ratio for all four systems with different compositions for different site occupancies and magnetic configurations. The red curves correspond to the minimum energy configurations and the blue curves are the ones with energies right above them. Solid curves with filled symbols indicate ground-state magnetic configurations and the dashed curves with open symbols are the ones with energies right above them, for each site-occupation configuration.

may see potential benefits in Ni-Mn-Sb systems with regard to functional properties associated with the volume-conserving martensitic transformation.

### E. Electronic structure

In this subsection, we try to understand the microscopic physics behind composition, site occupancy, and magnetic

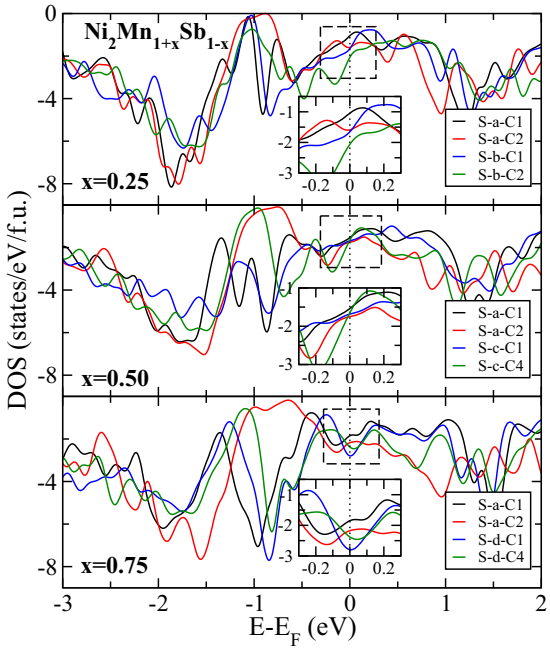


FIG. 5. The total spin down densities of states (DOS) for $Ni_2Mn_{1+x}Sb_{1-x}$ (sys1) ($x = 0.25,\ 0.50,\ 0.75$) in $L2_1$ phase with different site occupancies and magnetic configurations used in Fig. 4. The zero energy is set at Fermi energy ($E_F$). The insets show the zoomed view of total densities of states near Fermi level.

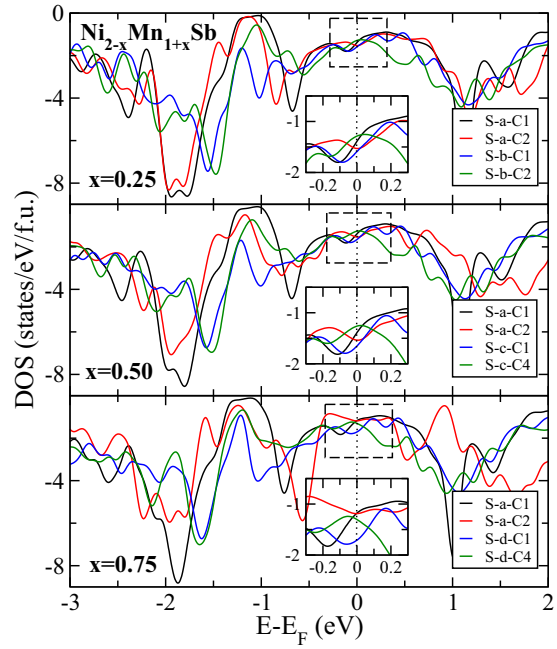


FIG. 6. The total spin down densities of states (DOS) of $Ni_{2-x}Mn_{1+x}Sb$ (sys2) ($x = 0.25,\ 0.50,\ 0.75$) in $L2_1$ phase with different site occupancies and magnetic configurations used in Fig. 4. The zero energy is set at Fermi energy ($E_F$). The insets show the zoomed view of total densities of states near Fermi level.

structure dependent stabilities of the austenite phase of Ni-Mn-Sb systems as discussed in the previous two subsections. We do this by computing the total and partial electronic densities of states of each compound with various compositions, normal and abnormal site occupancies, and different magnetic structures of Mn atoms. The total densities of states of the four systems in their respective minimum energy configurations at each composition for both $L2_1$ and tetragonal phases are shown in Fig. 2, Ref. [60]. The figures suggest that the stability of the austenite phase depends on the persistence of the pseudogap at around $-1.2$ eV in the minority band across compositions. It is well known for Ni-Mn-based shape memory systems that the occurrence of martensitic stability or the lack of it can be linked to the relative strengths of two factors: the Jahn-Teller effect manifested by substantial densities of states at the Fermi level and the covalent bonding due to Ni and the main group element manifested in a pseudogap in the occupied parts. We find that a competition between the strength of the Jahn-Teller instability and the strength of the covalent bond due to Ni $d$ and Sb $p$ minority states explains the phase stability in Ni-Mn-Sb too (for details, see description in Ref. [60].) To understand the dependencies of phase stability on composition, site occupancy, and magnetic structure, we analyze the electronic structures of the minority bands close to Fermi levels as shown in Figs. 5–8 for sys1 to 4, respectively. The densities of states are presented for those configurations for which the total energy curves were discussed in Fig. 4.

In Fig. 5, for sys1, we first compare the electronic structures corresponding to two magnetic structures C1 and C2 with the same normal site occupancy S-a. We find that with the magnetic configuration being C2, where Mn1 and Mn2 align parallel, the pseudogap in the minority band around $-1.2$ eV persists for all compositions and in fact becomes wider with increasing $x$. The structure at the Fermi level, on the other

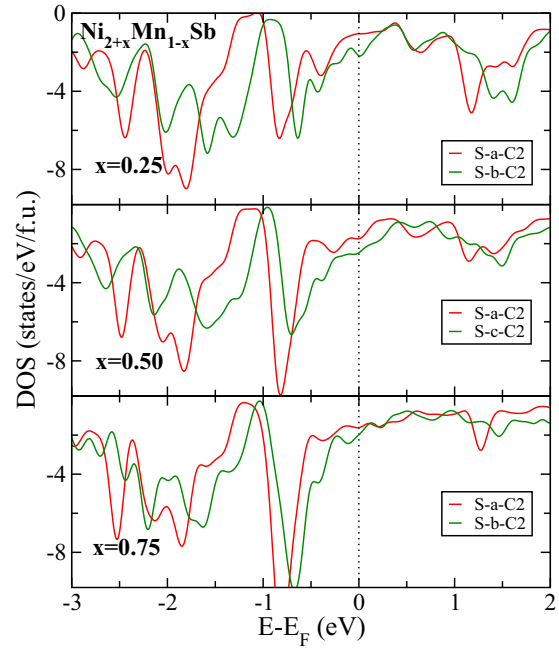


FIG. 7. The total spin down densities of states (DOS) of $Ni_{2+x}Mn_{1-x}Sb$ (sys3) ($x = 0.25,\ 0.50,\ 0.75$) in $L2_1$ phase with different site occupancies and magnetic configurations used in Fig. 4. The zero energy is set at Fermi energy ($E_F$).

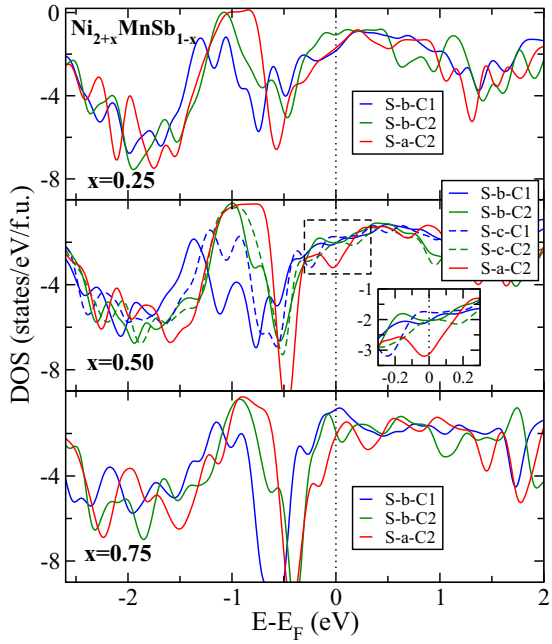


FIG. 8. The total spin down densities of states (DOS) of $Ni_{2+x}MnSb_{1-x}$ (sys4) ($x = 0.25, 0.50, 0.75$) in $L2_1$ phase with different site occupancies and magnetic configurations used in Fig. 4. The zero energy is set at Fermi energy ($E_F$). The inset shows the zoomed view of total densities of states near Fermi level for corresponding composition.

hand, has no significant difference due to changed magnetic configuration. This persisting pseudogap explains the stability of the $L2_1$ structure when two Mn atoms align parallel. The origin of this can be understood from the partial densities of states (Fig. 5, right panel, Ref. [60]). The pseudogap originating out of Ni and Sb hybridization could not be suppressed in C2 as, unlike C1, the Mn2 do not have states in this energy range. Next we analyze the effects of site-occupancy patterns by inspecting the S-b, S-c, and S-d densities of states. We find that for all abnormal configurations, irrespective of the magnetic structures, the pseudogap around $-1.2$ eV in stoichiometric $Ni_2MnSb$ gradually becomes narrower due to Ni1, Mn2 (Mn at Sb site), and Mn3 (Mn at Ni site) states in the down band (Fig. 6, Ref. [60]). Also a peak around $-0.3$ eV seen in $x = 0.25$ composition gradually shifts toward the Fermi level as $x$ increases and, finally, Fermi level falls on a peak in $x = 0.75$ which is mainly due to the states of Sb1, Ni1, and Mn3 atoms amplifying the Jahn-Teller instability in the system and driving it toward the martensitic transformations for both magnetic configurations as shown in Fig. 4. Thus, for sys1, for normal configurations, the Ni1 and Mn2 states, decrease the strength of covalent bonding with increase in Mn2, only when there is an antiparallel coupling between Mn1 and Mn2, bringing in the structural instability as the Jahn-Teller effect gains strength in relative sense. For abnormal site occupations, once again the hybridization between the spin-down bands of Ni and Mn atoms at various sites aligning antiparallel boosts the Jahn-Teller instability driving a phase transition.

In a similar way, we can infer that (i) for sys2, the changes in the hybridizations due to changes in site-occupancy configurations can induce instability in the $L2_1$ phase; the decisive factors being the deficiency of Sb at its own site and presence of antiparallel Mn-Mn interactions; (ii) the absence of Mn at any other site than its own in sys3 is the key factor behind the absence of any pronounced Jahn-Teller instability irrespective of configurations and thus behind the stability of the $L2_1$ phases throughout; and (iii) the hybridizations between Sb1, Ni1, and Ni2 minority bands in sys4 drive the system toward martensitic instability. The detailed discussion analyzing the features of electronic structures of sys2, sys3, and sys4 is given in Ref. [60].

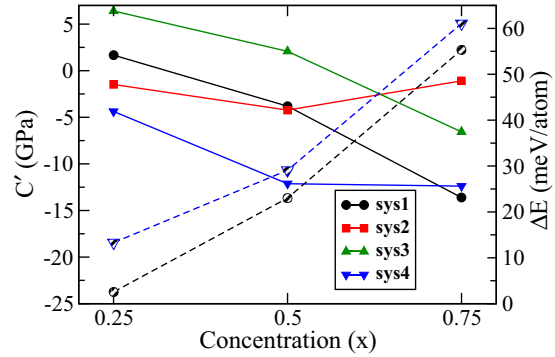


FIG. 9. The calculated shear elastic constant C′ in $L2_1$ phase as a function of concentration of excess atom $x$ for all four systems: $Ni_2Mn_{1+x}Sb_{1-x}$ (sys1), $Ni_{2-x}Mn_{1+x}Sb$ (sys2), $Ni_{2+x}Mn_{1-x}Sb$ (sys3), and $Ni_{2+x}MnSb_{1-x}$ (sys4) in their respective minimum energy configurations. The dashed lines represent the variation in $\Delta E$ (defined in Table III) with $x$.

### F. Elastic properties and predictor of $T_M$

Finally, in search of a predictor for $T_M$, we compute the composition dependence of elastic moduli. The results, apart from deciding on a predictor for $T_M$, provided insights into the mechanical properties and the nature of bonding in Ni-Mn-Sb. In case of Ni-Mn based Heusler alloys, the elastic modulus C′ in the austenite phase has been found to be a good predictor for $T_M$ [66–68]. The $(e/a)$ and $\Delta E$, the energy difference between $L2_1$ and tetragonal phases, are the other two quantities found to be good predictors in certain cases. In Fig. 9, we show the composition dependence of C′ for each of the four systems in $L2_1$ phases. Calculations are done in their respective minimum energy configurations. For sys1 and sys4, we find gradual softening of C′, indicating instability in the $L2_1$ phase. This is consistent with the results obtained from the total energy calculations. In fact, negative C′ at all compositions of sys4 indicates that the $L2_1$ structure is unstable across compositions. In sys1, a small positive C′ for $x = 0.25$ is consistent with a shallow minimum for $(c/a) \neq 1$ in the total energy curve. For sys2, C′ has little variation with composition while for sys3, we see positive C′ for $x = 0.25, 0.50$ which is consistent with the stable $L2_1$ phase at low temperature as seen from Fig. 3. The trends of $\Delta E$ shown in Fig. 9 for sys1 and sys4 are consistent with variations in C′; a decreasing (increasing) C′($\Delta E$) indicating increasing stability of the tetragonal phase and increasing value of $T_M$. For sys1, this is consistent with the experimental results where $T_M$ increases with $x$ [23]. It is also to be noted that

for sys1 and sys4, where our calculations predict martensitic transformations, $\Delta E$ increases with $(e/a)$ meaning that $T_M$ varies as $(e/a)$. Consequently, for Ni-Mn-Sb systems, both C′ and $(e/a)$ can be good predictors for $T_M$.

In Table II, Ref. [60], we show in detail the values of various elastic modulus for each compound. We calculated Pugh ratio ($G_v$/B) and Cauchy pressure ($C^P$) to get an idea about the brittleness and the nature of bonding in the compounds. Pugh ratio $G_v$/B [51,69], where $G_v$ is the isotropic shear modulus under Voigot formalism [50] related to the resistance of the material to plastic deformation, measures whether a material is more ductile or more brittle. Compounds having a Pugh ratio greater than 0.57 are considered to be more brittle. On the other hand, Cauchy pressure $C^P$ provides insight to the nature of bonding in a material with cubic symmetry [70]. A positive value of Cauchy pressure indicates the presence of more metallic bonding in the system while a negative value implies a stronger covalent bonding [71]. The tabulated values (see Table II, Ref. [60]) imply that Ni-Mn-Sb compounds are ductile in nature and the bonding is largely metallic.

## IV. SUMMARY AND CONCLUSIONS

In this paper, we have performed a comprehensive and systematic investigation into the roles of composition, site occupancies, and magnetic configurations affecting the structural stabilities in Ni and Mn-excess $Ni_2MnSb$ by *ab initio* calculations. We find that the site occupancy pattern and associated magnetic alignment of Mn atoms play the central role in destabilizing the high-temperature Heusler phase and consequently stabilizing a tetragonal martensite at low temperature. We find that unless the system is significantly Sb deficient, a martensitic transformation leading to the shape-memory effect and associated functional properties is difficult to realize unless the system stays in a metastable state due to the process of annealing or is grown by nonequilibrium methods. Our calculations for Mn-excess Sb-deficient systems reproduce the experimentally observed trends. The patterns in phase stability as obtained from our total energy calculations can be understood from the features in the densities of states in the minority spin bands. This paper helps understand the reason behind the experimentalist choice of Sb-deficient systems for observing functional properties like magnetocaloric effect in Ni-Mn-Sb. An important outcome of this work is the identification of $Ni_{2+x}MnSb_{1-x}$ as a potential new shape memory alloy where the martensitic transformation takes place even at high Sb composition. This input widens the scope of the experimentalists to explore functional properties in Ni-Mn-Sb systems. Shear modulus and electron to atom ratio $(e/a)$ both turn out to be good predictors of $T_M$ in Ni-Mn-Sb. The materials are also found to be ductile, which is an advantage for their commercial usages.

## ACKNOWLEDGMENTS

The authors gratefully acknowledge the Department of Science and Technology, India for the computational facilities under Grant No. SR/FST/P-II/020/2009 and IIT Guwahati for the PARAM supercomputing facility.

[1] K. Ullakko, J. Huang, C. Kantner, R. O'Handley, and V. Kokorin, Appl. Phys. Lett. **69**, 1966 (1996).
[2] S. J. Murray, M. Marioni, S. Allen, R. O'Handley, and T. A. Lograsso, Appl. Phys. Lett. **77**, 886 (2000).
[3] A. Sozinov, A. Likhachev, N. Lanska, and K. Ullakko, Appl. Phys. Lett. **80**, 1746 (2002).
[4] M. Chmielus, X. Zhang, C. Witherspoon, D. Dunand, and P. Müllner, Nat. Mater. **8**, 863 (2009).
[5] J. Marcos, A. Planes, L. Mañosa, F. Casanova, X. Batlle, A. Labarta, and B. Martínez, Phys. Rev. B **66**, 224413 (2002).
[6] F.-X. Hu, B.-g. Shen, J.-R. Sun, and G.-H. Wu, Phys. Rev. B **64**, 132412 (2001).
[7] T. Krenke, E. Duman, M. Acet, E. F. Wassermann, X. Moya, L. Mañosa, A. Planes, E. Suard, and B. Ouladdiaf, Phys. Rev. B **75**, 104414 (2007).
[8] M. Pasquale, C. P. Sasso, L. H. Lewis, L. Giudici, T. Lograsso, and D. Schlagel, Phys. Rev. B **72**, 094435 (2005).
[9] C. Biswas, R. Rawat, and S. Barman, Appl. Phys. Lett. **86**, 202508 (2005).
[10] V. Sharma, M. Chattopadhyay, K. Shaeb, A. Chouhan, and S. Roy, Appl. Phys. Lett. **89**, 222509 (2006).
[11] R. Kainuma, Y. Imano, W. Ito, Y. Sutou, H. Morito, S. Okamoto, O. Kitakami, K. Oikawa, A. Fujita, T. Kanomata *et al.*, Nature **439**, 957 (2006).
[12] R. Kainuma, Y. Imano, W. Ito, H. Morito, Y. Sutou, K. Oikawa, A. Fujita, K. Ishida, S. Okamoto, O. Kitakami *et al.*, Appl. Phys. Lett. **88**, 192513 (2006).
[13] V. Khovaylo, K. Skokov, O. Gutfleisch, H. Miki, R. Kainuma, and T. Kanomata, Appl. Phys. Lett. **97**, 052503 (2010).
[14] Z. Li, C. Jing, J. Chen, S. Yuan, S. Cao, and J. Zhang, Appl. Phys. Lett. **91**, 112505 (2007).
[15] M. Khan, I. Dubenko, S. Stadler, and N. Ali, Appl. Phys. Lett. **91**, 072510 (2007).
[16] K. Koyama, H. Okada, K. Watanabe, T. Kanomata, R. Kainuma, W. Ito, K. Oikawa, and K. Ishida, Appl. Phys. Lett. **89**, 182510 (2006).
[17] S. Yu, Z. Liu, G. Liu, J. Chen, Z. Cao, G. Wu, B. Zhang, and X. Zhang, Appl. Phys. Lett. **89**, 162503 (2006).
[18] M. K. Ray, B. Maji, M. Modak, and S. Banerjee, J. Magn. Magn. Mater. **429**, 110 (2017).
[19] N. V. Rama Rao, R. Gopalan, V. Chandrasekaran, and K. G. Suresh, Appl. Phys. A **99**, 265 (2010).
[20] Z. Han, D. Wang, C. Zhang, H. Xuan, B. Gu, and Y. Du, Appl. Phys. Lett. **90**, 042507 (2007).
[21] N. Duc, T. Thanh, N. Yen, P. Thanh, N. Dan, and T. Phan, J. Korean Phys. Soc. **60**, 454 (2012).
[22] M. Khan, N. Ali, and S. Stadler, J. Appl. Phys. **101**, 053919 (2007).
[23] W. J. Feng, J. Du, B. Li, W. J. Hu, Z. D. Zhang, X. H. Li, and Y. F. Deng, J. Phys. D **42**, 125003 (2009).
[24] S. Aksoy, M. Acet, E. F. Wassermann, T. Krenke, X. Moya, L. Manosa, A. Planes, and P. P. Deen, Philos. Mag. **89**, 2093 (2009).

[25] M. Khan, I. Dubenko, S. Stadler, and N. Ali, J. Phys.: Condens. Matter **20**, 235204 (2008).

[26] Q.-M. Hu, C.-M. Li, R. Yang, S. E. Kulkova, D. I. Bazhanov, B. Johansson, and L. Vitos, Phys. Rev. B **79**, 144112 (2009).

[27] V. V. Sokolovskiy, V. D. Buchelnikov, M. A. Zagrebin, P. Entel, S. Sahoo, and M. Ogura, Phys. Rev. B **86**, 134418 (2012).

[28] C.-M. Li, H.-B. Luo, Q.-M. Hu, R. Yang, B. Johansson, and L. Vitos, Phys. Rev. B **86**, 214205 (2012).

[29] A. Kundu and S. Ghosh, J. Phys.: Condens. Matter **30**, 015401 (2017).

[30] N. Lanska, O. Söderberg, A. Sozinov, Y. Ge, K. Ullakko, and V. Lindroos, J. Appl. Phys. **95**, 8074 (2004).

[31] A. Zayak, W. Adeagbo, P. Entel, and K. Rabe, Appl. Phys. Lett. **88**, 111903 (2006).

[32] T. Mehaddene, J. Neuhaus, W. Petry, K. Hradil, P. Bourges, and A. Hiess, Phys. Rev. B **78**, 104110 (2008).

[33] Y. Xin, Y. Li, C. B. Jiang, and H. B. Xu, Mater. Sci. Forum **475–479**, 1991 (2005).

[34] V. Kokorin and I. Osipenko, Phys. Met. Metallogr. (USSR) **67**, 173 (1989).

[35] C. Seguí, J. Pons, and E. Cesari, Acta Mater. **55**, 1649 (2007).

[36] V. Sánchez-Alarcos, V. Recarte, J. Pérez-Landazábal, and G. Cuello, Acta Mater. **55**, 3883 (2007).

[37] M. Khan, J. Jung, S. Stoyko, A. Mar, A. Quetz, T. Samanta, I. Dubenko, N. Ali, S. Stadler, and K. Chow, Appl. Phys. Lett. **100**, 172403 (2012).

[38] X. Ren and K. Otsuka, Mater. Sci. Forum **327–328**, 429 (2000).

[39] X. Ren, K. Otsuka, and T. Suzuki, J. Alloys Compd. **355**, 196 (2003).

[40] M. Stipcich, L. Mañosa, A. Planes, M. Morin, J. Zarestky, T. Lograsso, and C. Stassis, Phys. Rev. B **70**, 054115 (2004).

[41] A. Chakrabarti, C. Biswas, S. Banik, R. S. Dhaka, A. K. Shukla, and S. R. Barman, Phys. Rev. B **72**, 073103 (2005).

[42] J. Chen, Y. Li, J. Shang, and H. Xu, Appl. Phys. Lett. **89**, 231921 (2006).

[43] P. E. Blöchl, Phys. Rev. B **50**, 17953 (1994).

[44] G. Kresse and D. Joubert, Phys. Rev. B **59**, 1758 (1999).

[45] G. Kresse and J. Furthmüller, Phys. Rev. B **54**, 11169 (1996).

[46] J. P. Perdew, K. Burke, and M. Ernzerhof, Phys. Rev. Lett. **77**, 3865 (1996).

[47] F. D. Murnaghan, Proc. Natl. Acad. Sci. USA **30**, 244 (1944).

[48] L. Vitos, *Computational Quantum Mechanics for Materials Engineers: The EMTO Method and Applications, Engineering Materials and Processing* (Springer-Verlag, London, 2007).

[49] S. O. Kart and T. Cagın, J. Alloys Compd. **508**, 177 (2010).

[50] W. Voigt, Ann. Phys. Chem. **274**, 573 (1889).

[51] T. Roy, M. E. Gruner, P. Entel, and A. Chakrabarti, J. Alloys Compd. **632**, 822 (2015).

[52] T. Roy, D. Pandey, and A. Chakrabarti, Phys. Rev. B **93**, 184102 (2016).

[53] N. Rama Rao, J. A. Chelvane, V. Chandrasekaran, A. Morozkin, J. Lamsal, W. Yelon, R. Nirmala, K. Suresh, and S. Malik, J. Appl. Phys. **109**, 07A907 (2011).

[54] V. D. Buchelnikov, V. V. Sokolovskiy, M. A. Zagrebin, M. A. Tufatullina, and P. Entel, J. Phys. D **48**, 164005 (2015).

[55] V. V. Sokolovskiy, P. Entel, V. D. Buchelnikov, and M. E. Gruner, Phys. Rev. B **91**, 220409(R) (2015).

[56] G. Grimvall, Phys. Scr. **13**, 59 (1976).

[57] B. Johansson and P. Söderlind, Thermochim. Acta **218**, 145 (1993).

[58] B. L. Gyorffy, A. J. Pindor, J. Staunton, G. M. Stocks, and H. Winter, J. Phys. F: Met. Phys. **13**, 979 (1983).

[59] G. Grimvall, Phys. Rev. B **39**, 12300 (1989).

[60] See Supplemental Material at http://link.aps.org/supplemental/10.1103/PhysRevB.99.064112 for detailed discussions on contributions from lattice vibrations and chemical mixing toward total entropy, the results of total energy calculations with different directions of distortions for all systems with $x = 0.5$, total, and atom-projected densities of states for all systems considered and the results on various elastic constants.

[61] Y. Yang, S. Liu, H. Zhao, W. Yang, R. Wu, Q. Huang, D. Zhou, H. Du, C. Wang, Y. Yang *et al.*, Scr. Mater. **116**, 31 (2016).

[62] W. He, H. Huang, Z. Liu, and X. Ma, Intermetallics **90**, 140 (2017).

[63] Y. Ma, H. Hao, X. Liu, H. Luo, F. Meng, and H. Liu, Intermetallics **93**, 263 (2018).

[64] J. Du, Q. Zheng, W. J. Ren, W. J. Feng, X. G. Liu, and Z. D. Zhang, J. Phys. D **40**, 5523 (2007).

[65] A. Ghosh and K. Mandal, Appl. Phys. Lett. **104**, 031905 (2014).

[66] C.-M. Li, H.-B. Luo, Q.-M. Hu, R. Yang, B. Johansson, and L. Vitos, Phys. Rev. B **82**, 024201 (2010).

[67] H.-B. Luo, C.-M. Li, Q.-M. Hu, R. Yang, B. Johansson, and L. Vitos, Acta Mater. **59**, 971 (2011).

[68] O. Nittono and Y. Koyama, Jpn. J. Appl. Phys. **21**, 680 (1982).

[69] S. Pugh, London, Edinburgh, Dublin Philos. Mag. J. Sci. **45**, 823 (1954).

[70] D. Pettifor, Mater. Sci. Technol. **8**, 345 (1992).

[71] A. Kundu, S. Ghosh, and S. Ghosh, Phys. Rev. B **96**, 174107 (2017).